Available online at www.sciencedirect.com
SCIENCE DIRECT®
Journal of Sound and Vibration 283 (2005) 525–542
JOURNAL OF SOUND AND VIBRATION
www.elsevier.com/locate/jsvi

Numerical analysis of nonlinear rotor–seal system

J. Hua[a], S. Swaddiwudhipong[a,*], Z.S. Liu[b], Q.Y. Xu[c]

[a]*Department of Civil Engineering, National University of Singapore, Blk E1A 07-03, 1 Engineering Drive 2, 10 Kent Ridge Crescent, Singapore 119260, Singapore*
[b]*Computational Mechanics Division, Institute of High Performance Computing, 1 Science Park Road, #01-01 The Capricorn, Singapore 117528, Singapore*
[c]*Department of Engineering Mechanics, Xi'an Jiaotong University, Xi'an 710049, PR China*

Received 26 August 2003; received in revised form 18 February 2004; accepted 28 April 2004

Abstract

The seal characteristic is an important factor affecting the performance of the rotor system. The nonlinear model of the rotor–seal system is established using Muszynska's nonlinear seal forces. An efficient and high-precision direct integration scheme is presented based on the 2^N type algorithm for the computation of exponential matrices. The nonlinear phenomena in the unbalanced rotor–seal system are investigated using the adopted model and numerical integration method. The influence of the seal on the nonlinear characteristics of the rotor system is analyzed by the bifurcation diagrams and Poincaré maps. Various nonlinear phenomena in the rotor–seal system, such as periodic motion, double-periodic motion, quasi-periodic motion and Hopf bifurcation are investigated and the stability is judged by Floquet theory and bifurcation theorem. The influence of parameters on the critical instability speed of the balanced rotor–seal system is also included. The high-precision direct integration method is effectively applied to the nonlinear numerical analysis of the rotor–seal system. The scheme has high precision and a large time step may be adopted to save computing resources.

*Corresponding author.
E-mail addresses: cvehj@nus.edu.sg (J. Hua), cvesomsa@nus.edu.sg (S. Swaddiwudhipong).

0022-460X/$ - see front matter © 2004 Elsevier Ltd. All rights reserved.
doi:10.1016/j.jsv.2004.04.028

Nomenclature

m_d	mass of the disk
C_d	damping coefficient of shaft at disk
K_d	stiffness of shaft at disk
e	mass eccentricity of the disk
$\in$	eccentricity ratio of shaft at disk
ω	angular speed of the rotor
ω_c	critical instability speed of the rotor
s	nondimensional angular speed $(=\omega/\sqrt{K_d/m})$
t	time
$\bar{t}$	dimensionless time $(=\omega t)$
τ	time step
$(\cdot)$	derivative with respect to t
$(')$	derivative with respect to $\bar{t}$
g	gravity acceleration
ξ	radial clearance of the seal
γ	ratio of fluid circumferential average velocity to ω
K_s	stiffness of the seal
C_s	damping of the seal
m_s	inertia of the seal
R_s	radius of the seal
η	fluid dynamic coefficient
ζ	loss coefficient at the inlet
ΔP	reduction of the pressure of seal
l	length of the seal
v	axial fluid velocity
f	factor of friction
σ	gradient coefficient of loss of friction
R_a	Reynolds number of the axial flow
R_v	Reynolds number of the circumferential flow
λ	Floquet multiplier
n_0, m_0	empirical coefficients [2,3]
n_1	exponent (0.5–3)[2,3,19]
n_2	exponent (0–1.0)
x, y	displacements of the shaft centre
X, Y	nondimensional displacements $(=x/\xi, y/\xi)$
X', Y'	nondimensional velocities

Subscripts

d	disk
s	seal

1. Introduction

The performances of the rotor system are significantly influenced by the characteristics of the seal. It is imperative to understand the nonlinear behavior of the rotor–seal interaction in the design of the system. The seal forces, in many occasions, have caused damages to rotor–seal system though the values are less than the fluid film forces of the bearing [1]. With the increase in the rotating speed, medium pressure, the rotor flexibility and the decrease in the seal clearance, steam-excited problems become more crucial in system design. Research on the mechanism of fluid–solid interaction and the control of the steam-excited vibration in rotor–seal system has become one of the key issues for modern turbo-machinery design.

The dynamic coefficients of various seals have been extensively studied by linearizing the seal fluid forces around the equilibrium position of the rotor [2–5]. The determination of the dynamic coefficients of various seals was also investigated via experimental approaches [6–10]. The influences of the seal on the stability are carried out by experimental results and compared with theoretical values [11,12]. Marquette and Childs [13] adopted the extended three-control-volume model to study the dynamic characteristics of circumferentially grooved liquid seals. Research works are limited mainly to the calculation of the linear dynamic coefficients and the evaluation of stability. However, the nonlinear nature of the seal forces has to be considered when the

mechanism of the stability is explored. Noah and Sundararajan [14] discussed the limitations of the currently practiced linearized analysis and the significance of considering nonlinear effects in predicting the dynamic behavior of the rotating system. Compared to linear analysis, the nonlinear analysis of the rotor–seal system is still rare due to the difficulties in obtaining the analytical nonlinear model of seal fluid forces from the complicated fluid dynamics. To overcome this difficulty, a simple model of nonlinear fluid dynamic forces generated in the seal based on the results of a series of experiments, was proposed by Muszynska [15–18]. Subharmonic mechanism and the influence of unbalance for a single disk rotor–seal system are analyzed using Muszynska seal forces [19]. The nonlinear dynamic behavior of a rigid rotor supported on plain journal bearings was studied and the experimental confirmation of the theoretical results is later sought [20]. Ding et al. [21] investigated the Hopf bifurcation behavior of a symmetric rotor–seal system using Muszynska's seal force model. In the analysis, the instability from certain critical equilibrium positions for a perfectly balanced system is proved to be the result of Hopf bifurcation and only the supercritical type is found for a specific rotor system using Poore's algebraic criteria. The nonlinear dynamic phenomena and the bifurcation characteristics of the unbalanced rotor–seal system using Muszynska seal force model were also investigated by Hua et al. [22,23].

Constructing a suitable rotating seal model and selecting a suitable numerical scheme are critical to the success and efficiency of the solution process for this highly nonlinear dynamic system. The common disadvantages of some general numerical methods to solve nonlinear structural dynamic equations are their sensitivity to time step and low precision. The precise integration method proposed by Zhong [24,25] can be used to solve this class of nonlinear equations with high precision. The scheme permits larger size of time step compared to other existing methods and hence generally lower computational efforts [23]. In this paper, the nonlinear dynamic characteristics of rotor–seal system are studied using Muszynska seal force model. In order to improve the computing efficiency and the precision of the solutions, the precise direct integration method is adopted in the time-marching algorithm. The influence of the seal characteristics on the nonlinear phenomena of the rotor system and the stability of periodic solution are investigated using Floquet theory and bifurcation theorem. The bifurcation diagrams and Poincaré maps are presented to illustrate the variation of periodic motion of the system. Several nonlinear motions in the system such as periodic motion, double-periodic motion, quasi-periodic motion, Hopf bifurcation and jump phenomenon are demonstrated in more details through numerical studies.

2. Unbalanced rotor–seal system

The equations governing the motion of the single disk rotor–seal system shown in Fig. 1 are expressed as

$$\begin{bmatrix} m_d & 0 \\ 0 & m_d \end{bmatrix} \begin{Bmatrix} \ddot{x} \\ \ddot{y} \end{Bmatrix} + \begin{bmatrix} C_d & 0 \\ 0 & C_d \end{bmatrix} \begin{Bmatrix} \dot{x} \\ \dot{y} \end{Bmatrix} + \begin{bmatrix} K_d & 0 \\ 0 & K_d \end{bmatrix} \begin{Bmatrix} x \\ y \end{Bmatrix} = \begin{Bmatrix} F_x \\ F_y \end{Bmatrix} + \begin{Bmatrix} 0 \\ -m_d g \end{Bmatrix} + m_d e\omega^2 \begin{Bmatrix} \cos\ \omega t \\ \sin\ \omega t \end{Bmatrix}, \tag{1}$$

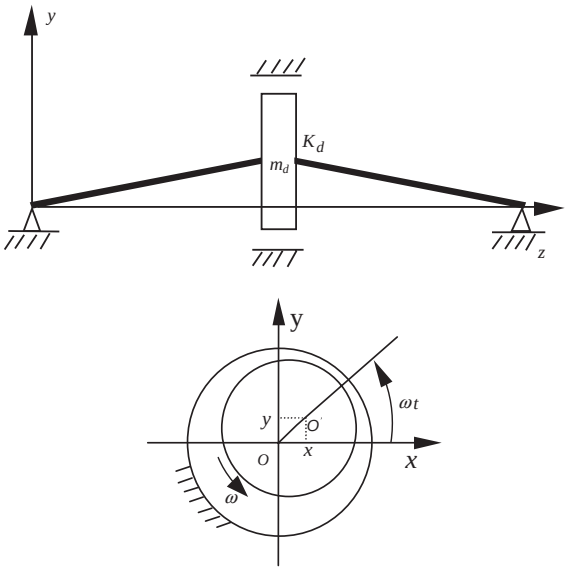

Fig. 1. Rotor–seal system.

where m_d is the mass of disk, C_d the damping coefficient of the shaft at disk, K_d the stiffness of the shaft at disk, x, y the displacements of the shaft center, g the gravity acceleration, e the mass eccentricity of the disk, ω the angular speed of the rotor, t the time and $(\dot{})$ representing derivative with respect to t.

The expressions for the Muszynska seal forces, F_x and F_y, acting on the disk and various parameters influencing the forces and motion are given in Appendix A.

Introducing the following nondimensional transform:

$$X = x/\xi, \quad Y = y/\xi, \quad \bar{t} = \omega t, \tag{2a–c}$$

$$\dot{x} = \omega\xi X', \quad \ddot{x} = \omega^2\xi X'', \tag{2d,e}$$

$$\dot{y} = \omega\xi Y', \quad \ddot{y} = \omega^2\xi Y'', \tag{2f,g}$$

where ξ is the radial clearance of the seal.

Substituting the expressions for the Muszynska seal forces in Eq. (1) in view of Eqs. (2a)–(2g) leads to the following set of governing equations:

$$\begin{bmatrix} 1 & 0 \\ 0 & 1 \end{bmatrix} \begin{Bmatrix} X'' \\ Y'' \end{Bmatrix} + \begin{bmatrix} C_1 & C_2 \\ -C_2 & C_1 \end{bmatrix} \begin{Bmatrix} X' \\ Y' \end{Bmatrix} + \begin{bmatrix} K_1 & K_2 \\ -K_2 & K_1 \end{bmatrix} \begin{Bmatrix} X \\ Y \end{Bmatrix} = \begin{Bmatrix} 0 \\ G \end{Bmatrix} + \rho^2 \begin{Bmatrix} \cos\ t \\ \sin\ t \end{Bmatrix}, \tag{3}$$

in which

$$K_1 = \frac{K_d + K_s - \gamma^2\omega^2 m_s}{m\omega^2}, \quad K_2 = \frac{\gamma C_s}{m\omega}, \tag{4a,b}$$

$$C_1 = \frac{C_d + C_s}{m\omega}, \quad C_2 = \frac{2\gamma m_s}{m}, \tag{5a,b}$$

$$G = -m_d g/(m\omega^2\xi), \quad m = m_d + m_s, \tag{6a,b}$$

$$\rho^2 = m_d r/m\xi. \tag{7}$$

Expressions for parameters, K_s, m_s, C_s and γ are included in Appendix A.

The unbalanced rotor–seal system is nonautonomous. When the values of the system parameters vary, the double-periodic motion and quasi-periodic motion may be excited by the imbalance of the rotor while the periodic motion will lose its stability.

The high-precision direct integration method is adopted to determine the periodic motion while the Floquet transition matrix method for its stability.

As rotor speed varies, three types of instability may occur [26,27]:

(1) If the leading multiplier crosses the unit circle at (–1,0), the periodic motion becomes unstable and a double-periodic motion develops.
(2) If the leading multiplier crosses the unit circle at (1,0), a saddle-node type instability occurs and the usual jump in the response curve manifested.
(3) The unit circle is crossed at a pair of complex-conjugate multipliers. The periodic motion becomes unstable and bifurcates into a quasi-periodic motion having two irrational fundamental frequencies.

If the mass eccentricity of the disk, e, vanishes, the rotor is well balanced and the system is autonomous. As the system parameters vary, the Hopf bifurcation may occur resulting in the periodic motion. The stability of the equilibrium position can be determined by calculating the eigenvalues of the Jacobean matrix of the state equation at the equilibrium position. If all the real parts of the eigenvalues are negative, the equilibrium point is stable. If any one of the real parts is positive, the equilibrium point is unstable [26].

3. High-precision direct time integration

The structural dynamic equations can be written as

$$\mathbf{M}\ddot{\mathbf{x}} + \mathbf{C}\dot{\mathbf{x}} + \mathbf{K}\mathbf{x} = \mathbf{f}(t, \mathbf{x}, \dot{\mathbf{x}}) \tag{8}$$

with the following initial conditions:

$$\mathbf{x}(t_0) = \mathbf{x}_0, \quad \dot{\mathbf{x}}(t_0) = \dot{\mathbf{x}}_0. \tag{9a,b}$$

Introducing $\mathbf{p} = \mathbf{M}\dot{\mathbf{x}} + \mathbf{C}\mathbf{x}/2$, Eq. (8) becomes

$$\dot{\mathbf{U}} = \mathbf{H}\mathbf{U} + \mathbf{q}, \quad \mathbf{U}(\mathbf{0}) = \mathbf{U}_0, \tag{10a,b}$$

where

$$\mathbf{U} = \begin{Bmatrix} \mathbf{x} \\ \mathbf{p} \end{Bmatrix}, \quad \mathbf{q} = \begin{Bmatrix} \mathbf{0} \\ \mathbf{f} \end{Bmatrix}^{\mathrm{T}}, \quad \mathbf{H} = \begin{bmatrix} -\frac{1}{2}\mathbf{M}^{-1}\mathbf{C} & \mathbf{M}^{-1} \\ \frac{1}{4}\mathbf{C}\mathbf{M}^{-1}\mathbf{C} - \mathbf{K} & -\frac{1}{2}\mathbf{C}\mathbf{M}^{-1} \end{bmatrix}. \tag{11a–c}$$

The general solutions of the homogeneous equations $\dot{\mathbf{U}} = \mathbf{H}\mathbf{U}$ can be expressed as

$$\mathbf{U} = \exp(\mathbf{H}t)\mathbf{U}_0. \tag{12}$$

Then

$$\mathbf{U}(\tau) = \exp(\mathbf{H}\tau)\mathbf{U}_0 = \mathbf{T}\mathbf{U}_0. \tag{13}$$

The derivation of transformation matrix $\mathbf{T}$ is given in Appendix B.

The non-homogeneous term, $\mathbf{q}$, in Eqs. (10a), is assumed to be linear in each time step (t_k, t_{k+1}), and hence

$$\dot{\mathbf{U}} = \mathbf{H}\mathbf{U} + \mathbf{q}_0 + \mathbf{q}_1(t - t_k), \tag{14}$$

$$\mathbf{q}_0 = \mathbf{q}(\mathbf{U}_{k-1}, t_{k-1}), \quad \mathbf{q}_1 = \frac{\mathrm{d}}{\mathrm{d}t}\mathbf{q}(\mathbf{U}_{k-1}, t_{k-1}). \tag{15a,b}$$

Note that at time $t = t_k$, $\mathbf{U} = \mathbf{U}_k$ and $\mathbf{U}_k$ can be evaluated from

$$\mathbf{U}_k = \mathbf{T}\mathbf{U}_{k-1} + \mathbf{T}\mathbf{H}^{-1}(\mathbf{q}_0 + \mathbf{H}^{-1}\mathbf{q}_1) - \mathbf{H}^{-1}(\mathbf{U}_0 + \mathbf{H}^{-1}\mathbf{q}_1 + \mathbf{q}_1\tau). \tag{16}$$

The following recursion is adopted to improve further the precision of the results:

$$\mathbf{U}_k = \mathbf{T}(t_k - t_{k-1})\mathbf{U}_{k-1} + f_{k-1}\,\frac{t_k - t_{k-1}}{2}\sum_{j=1}^{\overline{N}} A(t_j)\mathbf{T}(t_j), \tag{17}$$

where A, t_j are the weighting and location of the time-integration point of Gauss quadrature, respectively [23].

Consider the following simple example:

$$\begin{bmatrix} 2 & 0 \\ 0 & 1 \end{bmatrix}\begin{Bmatrix} \ddot{x} \\ \ddot{y} \end{Bmatrix} + \begin{bmatrix} 6 & -2 \\ -2 & 4 \end{bmatrix}\begin{Bmatrix} x \\ y \end{Bmatrix} = \begin{Bmatrix} 0 \\ 10 \end{Bmatrix} \tag{18}$$

with the following initial conditions:

$$x(0) = y(0) = 0, \quad \dot{x}(0) = \dot{y}(0) = 0. \tag{19}$$

Its theoretical solutions are

$$\begin{Bmatrix} x \\ y \end{Bmatrix} = \frac{1}{3}\begin{bmatrix} 1 & \sqrt{2}/2 \\ 1 & -\sqrt{2} \end{bmatrix}\begin{bmatrix} 5(1 - \cos\sqrt{2}t) \\ 2\sqrt{2}(-1 + \cos\sqrt{5}t) \end{bmatrix}. \tag{20}$$

The parameters adopted in Newmark time-marching scheme are $\alpha = 0.25$ and $\beta = 0.5$ while $\theta = 1.4$ is used for Wilson-θ method. The values of x at various time steps obtained from three time-marching schemes are presented in Table 1. It is observed that results obtained from the high precision direct time integration agree well with theoretical solutions. For the same size of time step, the high precision direct time-integration method produces results with higher accuracy than these obtained from the other two time-marching schemes, namely, Wilson-θ method and Newmark time-marching scheme. A similar conclusion can also be obtained for y.

Zhong [24] discussed the accuracy of the precise integration method and pointed out that the numerical results of the precise integration scheme are actually those of precise solution for

Table 1
Comparison of results of x from various time-marching schemes

Time (s)	Wilson θ	Newmark	Present study	Theoretical solution
0.280	0.006	0.0067	0.002514	0.002515
0.840	0.196	0.189	0.175594	0.175595
1.12	0.49	0.485	0.486026	0.486026
1.68	1.54	1.58	1.656964	1.656965
1.96	2.16	2.23	2.338202	2.338202
2.24	2.67	2.76	2.860814	2.860814
2.52	2.92	3.00	3.051708	3.051709
2.8	2.82	2.85	2.805723	2.805723
3.08	2.33	2.28	2.130584	2.130584
3.36	1.54	1.40	1.157226	1.157226

Table 2
Parameters and values used in numerical studies

Case	n	γ	b	n_0	m_0	z	δ (m)	e (m)
1	2.0	0.3	0.5	0.079	0.25	0.1	0.0025	0.0002
2	2.2	0.4	0.3	0.079	0.25	0.1	0.0025	0.0002

time-invariant system. Lin [25] obtained accurate responses to each harmonic component even for very large time steps using the high-precision direct time-integration scheme.

4. Numerical results and discussions

A computer program based on the proposed approach was developed to evaluate the dynamic responses of the rotor–seal system. The bifurcation diagrams are presented to show the variation course of the motion of the system. The diagram is constructed by presenting the dimensionless displacement on Poincaré section, X, at various nondimensional angular speed, $s = \omega/\sqrt{K_d/m}$.

4.1. Case 1

The values of the parameters adopted for case 1 are tabulated in Table 2. The bifurcation diagram of the rotor center is established and the results are shown in Fig. 2. It can be observed that the response of the system varies with the dimensionless angular speed s. The system possesses the periodic motion from the beginning. The periodic motion with the leading Floquet multiplier whose modulus is less than one is stable. Then at a speed of $s = 0.9$, the leading Floquet multiplier $\lambda_1 = 1.0741$ crosses the unit circle at (1,0) and the jump phenomenon of the response occurs indicating that the system becomes unstable and hence sensitive to the rotating speed in the neighborhood of this speed (Fig. 2).

Increasing the rotating speed sequentially, a synchronous stable periodic motion reappears with the leading Floquet multiplier whose modulus is less than one. Fig. 3 depicts the stable periodic

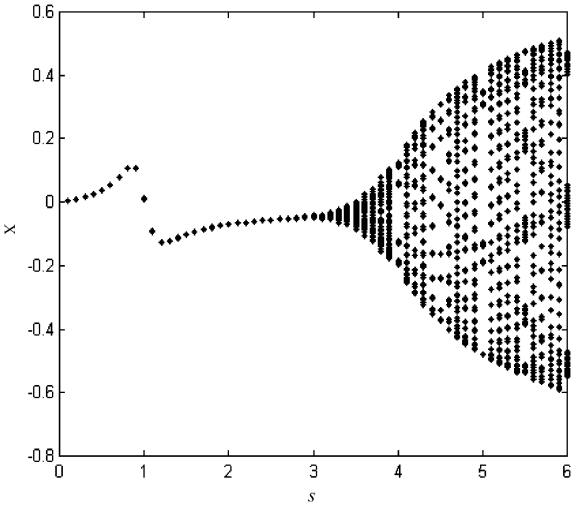

Fig. 2. Bifurcation diagram of rotor center for case 1.

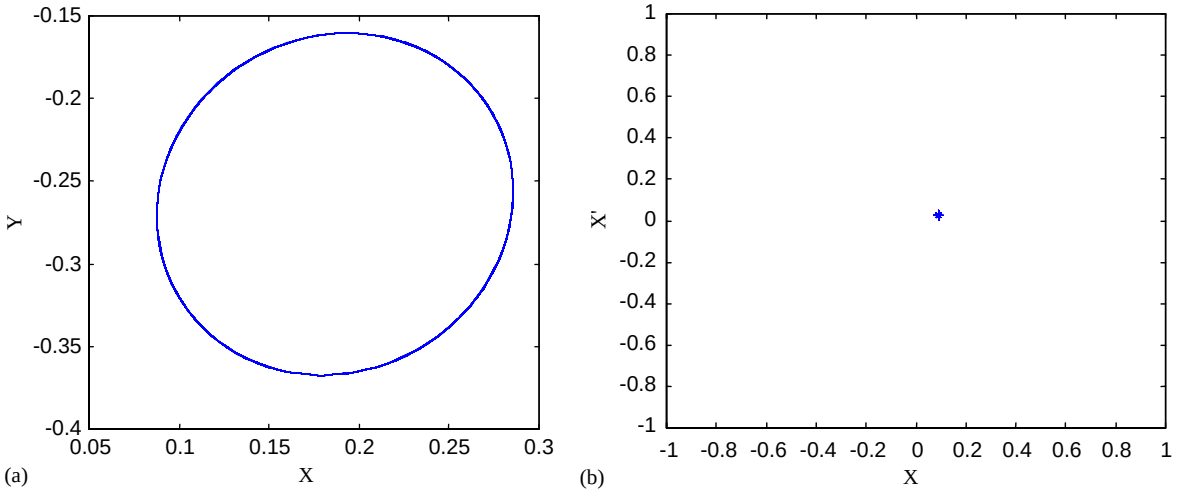

Fig. 3. Periodic motion for case 1 at $s = 1.5$: (a) orbit of rotor center, (b) Poincaré map.

motion with the Floquet multipliers of $\lambda = (-0.3439 + 0.7011\mathrm{i}, -0.3439 - 0.7011\mathrm{i}, -0.0012 + 0.0084\mathrm{i}, -0.0012 - 0.0084\mathrm{i})$ at $s = 1.5$. At $s = 3.07$, there is a leading Floquet multiplier $\lambda_1 = -1.000$ whose modulus is equal to one, viz. the critical point at which the periodic motion loses its stability and bifurcate into double-periodic motion. As the speed is increased to $s = 3.11$, Fig. 4 shows the appearance of the double periodic with the Floquet multipliers of $\lambda = (-1.04936, -0.06868 + 0.00631\mathrm{i}, -0.06868 - 0.00631\mathrm{i}, -0.91485)$ and the leading Floquet multiplier passing through the unit circle at point (–1,0). There exist two isolated points on Poincaré map corresponding to the double-periodic bifurcation. This implies that the half frequency whirl of the rotor–seal system will occur in the vicinity of this speed. As s exceeds 3.4, quasi-periodic

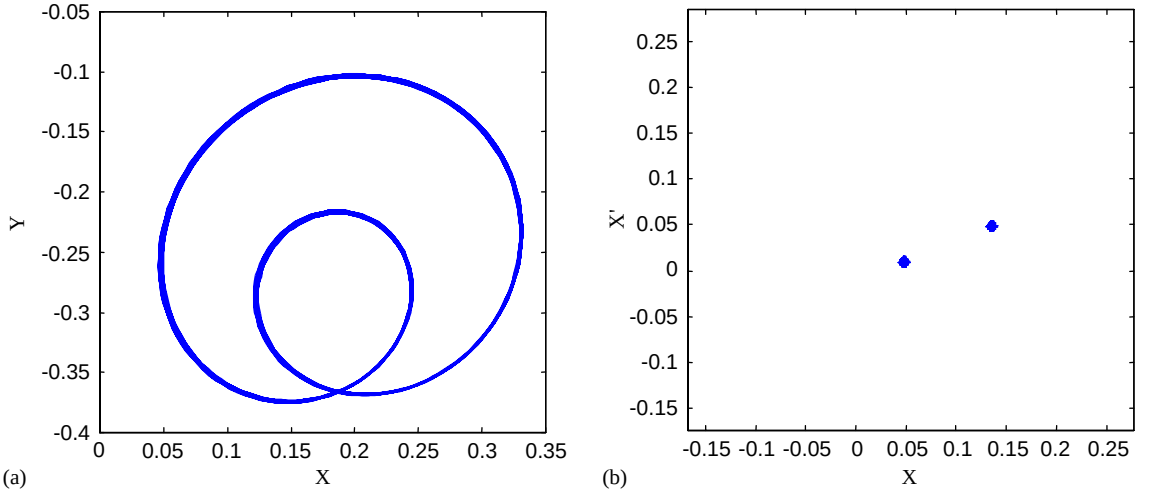

Fig. 4. Double periodic motion for case 1 at $s = 3.11$: (a) orbit of rotor center, (b) Poincaré map.

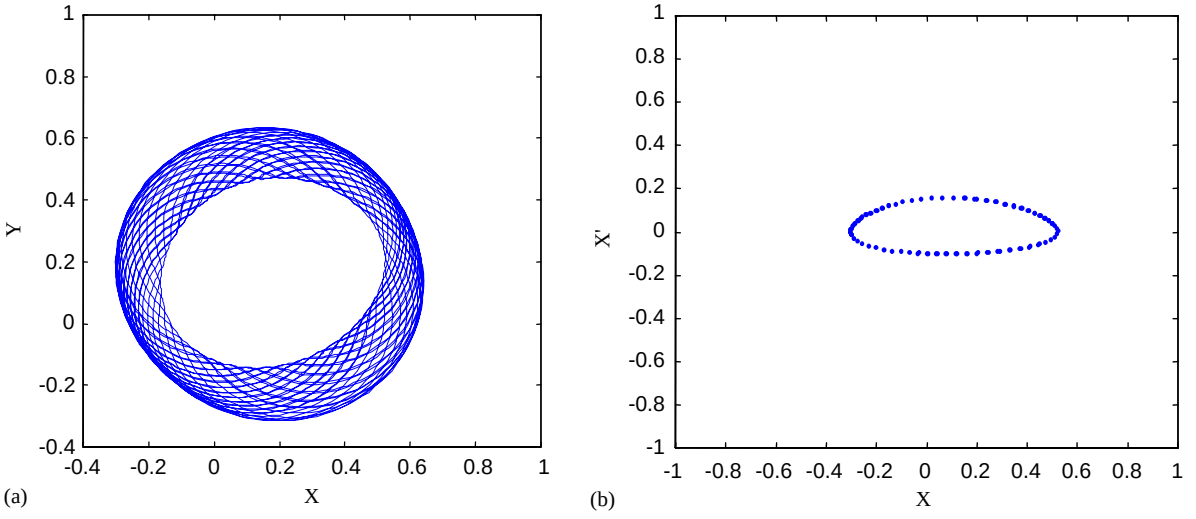

Fig. 5. Quasi-periodic motion for case 1 at $s > 3.4$: (a) orbit of rotor center, (b) Poincaré map.

motion appears and a close curve is observed on Poincaré map as shown in Fig. 5. The $\frac{1}{4}$ and $\frac{1}{5}$ subharmonic motions at $s = 4.0$ and 5.0, respectively, are illustrated in Figs. 6 and 7. As the rotating speed increases further, more complex motions are expected.

4.2. Case 2

Values of the parameters adopted for case 2 are also given in Table 2. The bifurcation diagram of the system is shown in Fig. 8(a) while details for s varying from 2.6 to 3.0 are magnified and illustrated in Fig. 8(b). Fig. 9(a) shows the orbit of triple-periodic motion while three isolated

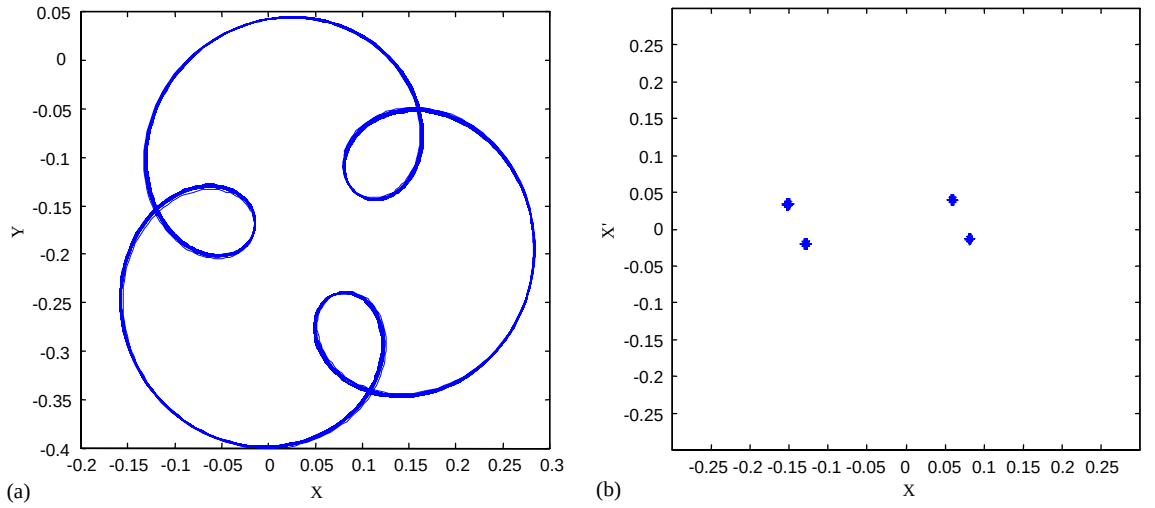

Fig. 6. 1/4 subharmonic motion for case 1 at $s = 4.0$: (a) orbit of rotor center, (b) Poincaré map.

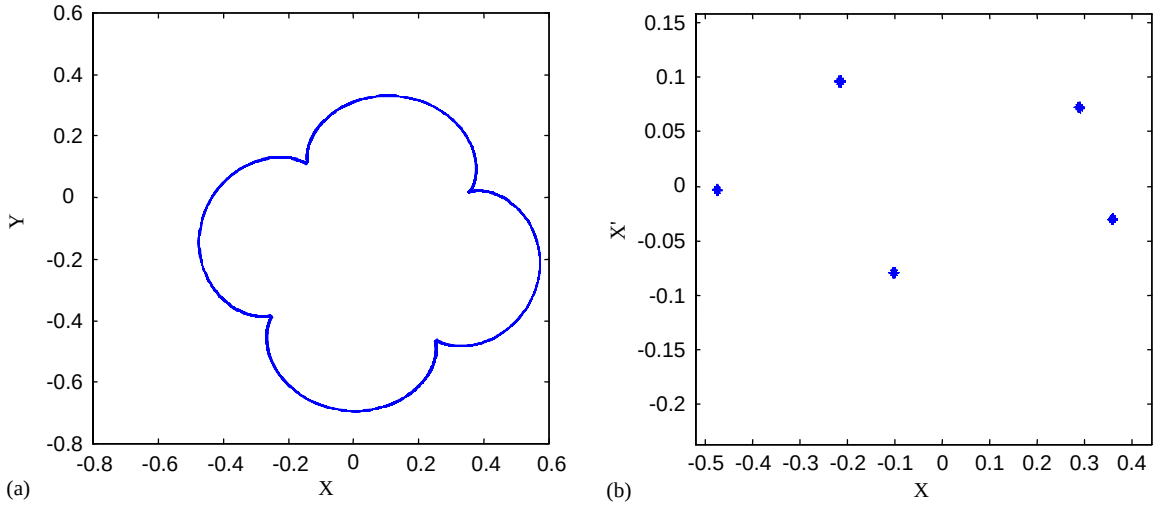

Fig. 7. 1/5 subharmonic motion for case 1 at $s = 5.0$: (a) orbit of rotor center, (b) Poincaré map.

points on Poincaré map are depicted in Fig. 9(b). The appearance of a triple-periodic motion implies that chaos exists theoretically in the vicinity of $s = 3.0$. Rigorous study on chaotic motion can be made by Lyapunov exponents or by power spectra of time series of the system responses. An attractor for a dissipative system with one or more positive Lyapunov exponents is said to be strange or chaotic [28].

Fig. 10 shows the bifurcation diagram of the system with an increase in the unbalanced value from $e = 0.0002$ to 0.0003 m while the other parameters are kept unchanged. Comparison between Figs. 8(a) and 10 reveals that the instability speed of the latter is higher than that of the former.

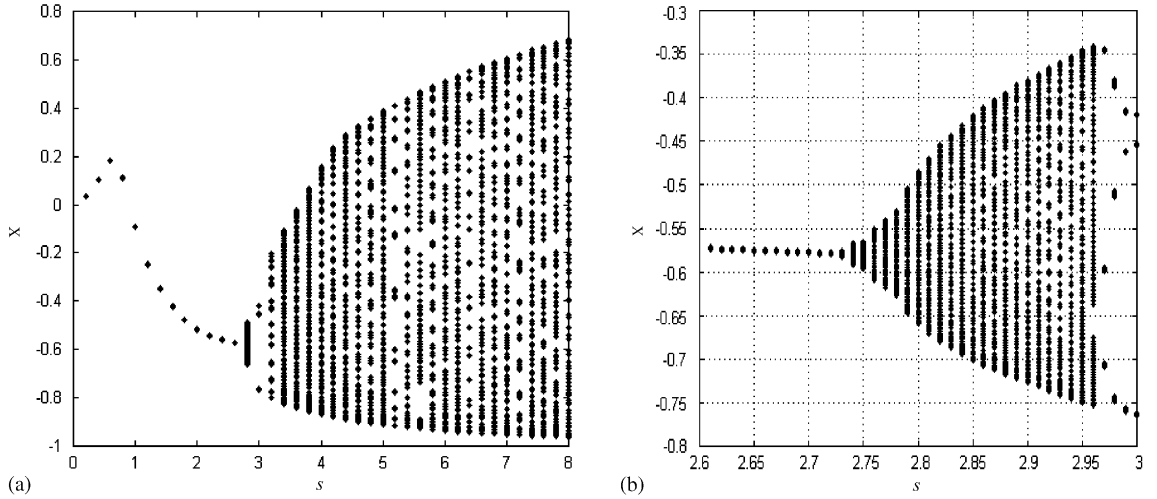

Fig. 8. Bifurcation diagram of rotor center for case 2: (a) bifurcation, (b) zoom of (a) at $s = 2.6 - 3.0$.

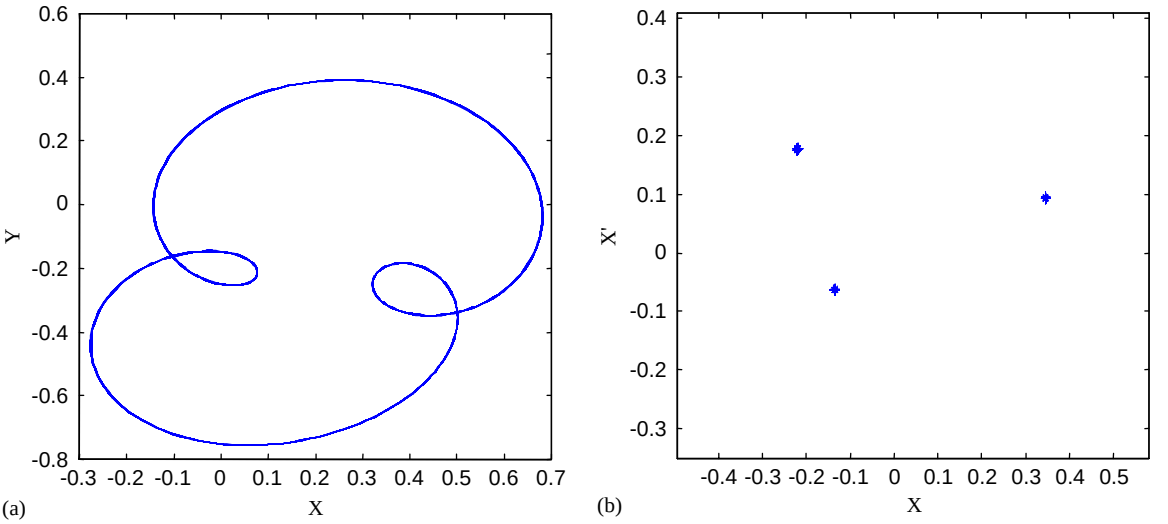

Fig. 9. 1/3 subharmonic motion for case 2 at $s = 3.0$: (a) orbit of rotor center, (b) Poincaré map.

This indicates that proper setup unbalance values may improve the stability of the rotor–seal system. Fig. 11 shows the $\frac{1}{8}$ subharmonic motion occurs at $s = 4.5$.

4.3. Case 3

The values of the parameters used in this case are the same as those in case 1 with the exception that the value of e vanishes resulting in the balanced rotor–seal system.

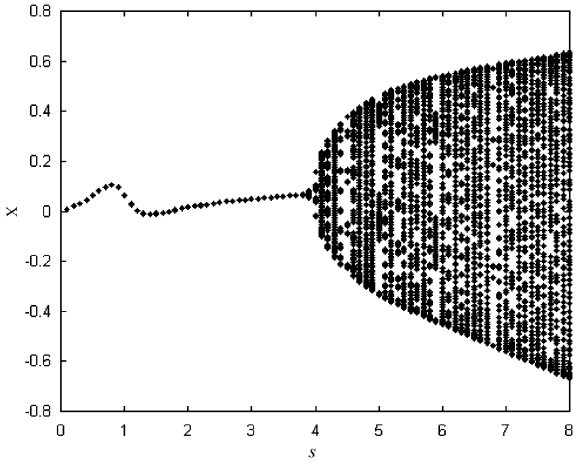

Fig. 10. Bifurcation diagram of rotor center for $e = 0.0003$ m.

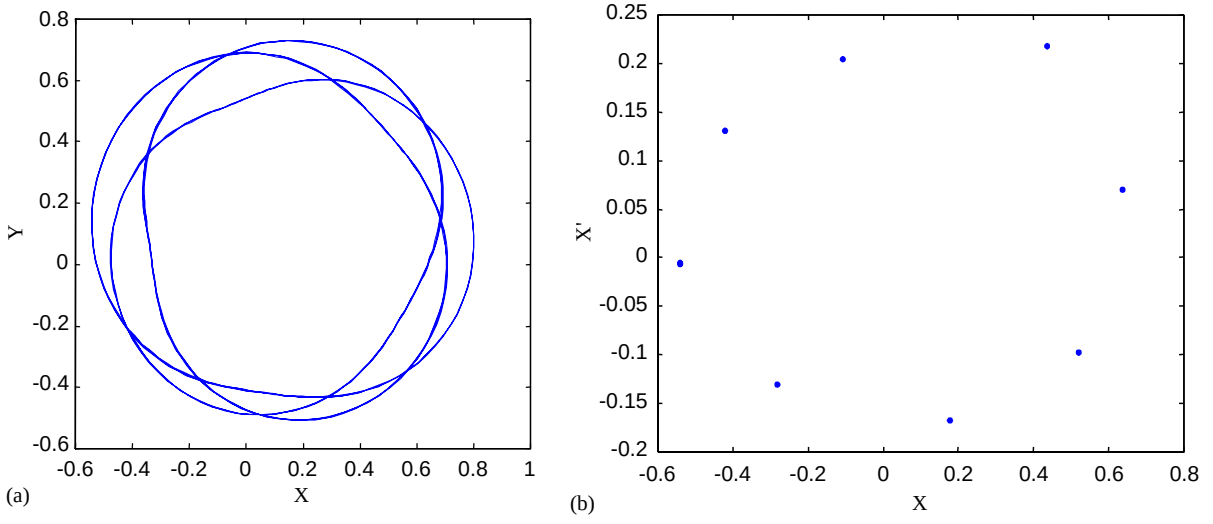

Fig. 11. 1/8 subharmonic motion for $e = 0.0003$ m at $s = 4.5$: (a) orbit of rotor center, (b) Poincaré map.

At the speed of $\omega = 283.8$ rad/s, the equilibrium point of the system is (0.03561, –0.18967) and the eigenvalues of the Jacobean matrix are (–0.03895 + 0.49446i, –0.03895 –0.49446i, –0.13441 + 0.46078i, –0.13441–0.46078i). Since all the real parts are negative, the equilibrium point is stable. The orbit of the rotor center is given in Fig. 12 including the transient course and it can be seen that the equilibrium position is asymptotically stable.

As the angular speed, ω, increases to 505.8 rad/s, the eigenvalues of the Jacobean matrix become (0.0000 + 0.27290i, 0.0000–0.27290i, –0.07492 + 0.27065i,–0.07492–0.27065i). Since the

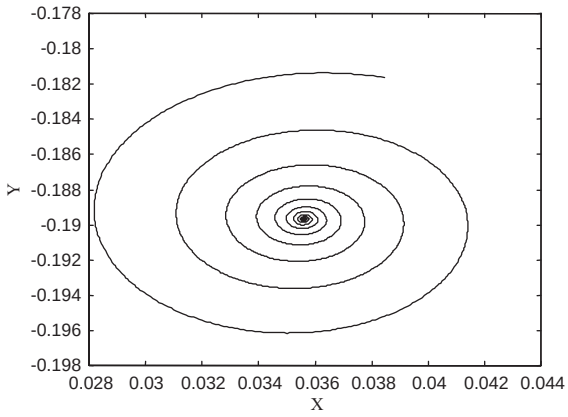

Fig. 12. Orbit the rotor center at $\omega = 283.84$ rad/s for case 3.

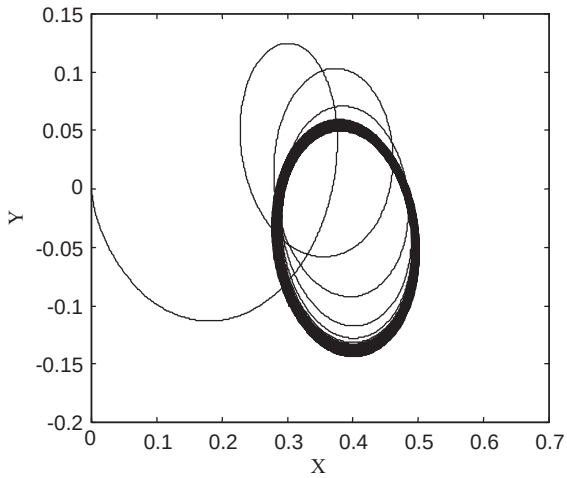

Fig. 13. Orbit the rotor center at $\omega = 520.1$ rad/s for case 3.

Jacobean matrix has two nonzero, purely imaginary eigenvalues, the Hopf bifurcation occurs. At the speed of $\omega = 520.1$ rad/s, the Jacobean matrix has a pair of complex-conjugate eigenvalues with positive real parts, viz. the equilibrium point loses its stability. The orbit of the rotor center as given in Fig. 13 shows that the orbit finally approaches a limit cycle. This type of instability is normally referred to as the oil whirl and the speed which causes this phenomenon is defined as the threshold speed.

The influences of the values of the parameters on the critical instability speed ω_c can also be analyzed. Figs. 14–16 demonstrated that the values of ω_c decrease gradually as these of m_d, γ_0, or n_1 increase. However, ω_c varies directly with ξ as demonstrated in Fig. 17.

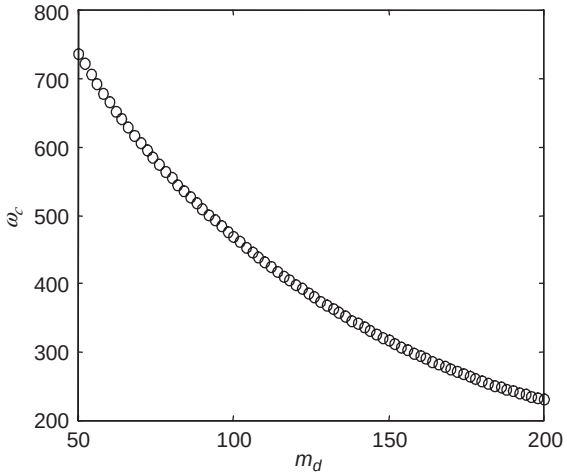

Fig. 14. Relationship between critical instability speed, ω_c, and mass of disk, m_d, for case 3.

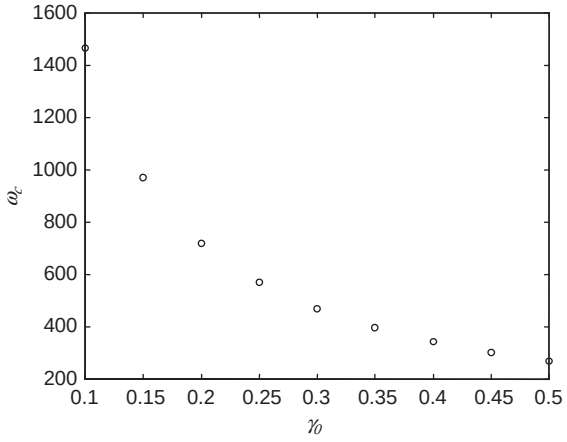

Fig. 15. Relationship between critical instability speed, ω_c, and the coefficient, γ_0, for case 3.

5. Conclusions

The nonlinear model of rotor–seal system is established using Muszynska seal forces. An efficient and high-precision direct integration scheme is adopted to investigate the nonlinear behavior of the unbalanced rotor–seal system. The bifurcation diagrams and Poincaré maps are presented to depict the influence of the seal on the nonlinear characteristics of the rotor system while the stability of the periodic motion are determined by Floquet multiplier. Several possible complex motions in the rotor–seal system including periodic motion, double-periodic motion, quasi-periodic motion and Hopf bifurcation are illustrated through several numerical examples. The balanced case is also provided and the influence of parameters on the critical instability speed

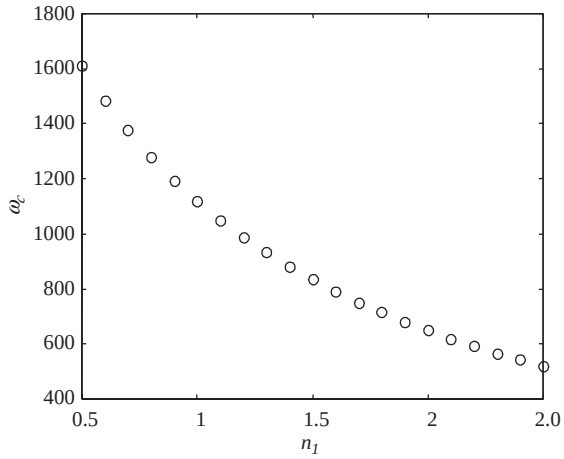

Fig. 16. Relationship between critical instability speed, ω_c, and exponent, n_1, for case 3.

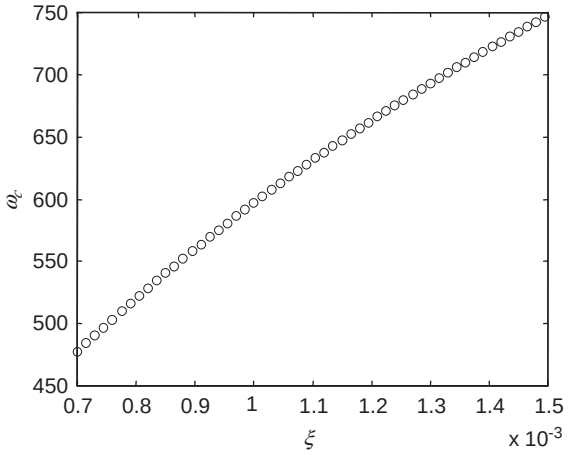

Fig. 17. Relationship between critical instability speed, ω_c, and radial clearance, ξ, for case 3.

is described. The study also demonstrates that the proposed high-precision direct integration method can be effectively applied to the nonlinear numerical analysis of rotor–seal system with higher order of accuracy and less computational effort.

Appendix A. Muszynska seal forces

Based on a series of experimental results, Muszynska [15–18] proposed the following expressions for seal fluid dynamic forces:

$$\begin{Bmatrix} F_x \\ F_y \end{Bmatrix} = -\begin{bmatrix} K_s - m_s\gamma^2\omega^2 & \gamma\omega C_s \\ -\gamma\omega C_s & K_s - m_s\gamma^2\omega^2 \end{bmatrix} \begin{Bmatrix} x \\ y \end{Bmatrix} - \begin{bmatrix} C_s & 2m_s\gamma\omega \\ -2m_s\gamma\omega & C_s \end{bmatrix} \begin{Bmatrix} \dot{x} \\ \dot{y} \end{Bmatrix} - \begin{bmatrix} m_s & 0 \\ 0 & m_s \end{bmatrix} \begin{Bmatrix} \dot{x} \\ \dot{y} \end{Bmatrix}, \tag{A.1}$$

where

$$\gamma = \gamma_0(1- \in)^{n_2}, \quad 0<n_2<1, \ \ \gamma_0<0.5, \tag{A.2}$$

$$K_s = K_0(1-\in^2)^{-n_1}, \quad C_s = C_0(1-\in^2)^{-n_1}, \tag{A.3}$$

$$\in= (x^2+y^2)^{1/2}/\xi, \quad K_0 = \mu_3\mu_0, \tag{A.4}$$

$$C_0 = \mu_1\mu_3\Lambda, \quad m_s = \mu_2\mu_3\Lambda^2, \tag{A.5}$$

$$\mu_0 = \frac{2\sigma^2}{1+\xi+2\sigma}\,E(1-m_0), \quad \mu_1 = \frac{2\sigma^2}{1+\xi+2\sigma}\left[\frac{E}{\sigma}+\frac{B}{2}\left(\tfrac{1}{6}+E\right)\right], \tag{A.6}$$

$$\mu_2 = \frac{\sigma(\frac{1}{6}+E)}{1+\zeta+2\sigma}, \quad \mu_3 = \frac{\pi R_s\Delta P}{f}, \tag{A.7}$$

$$\Lambda = \frac{l}{v}, \quad \sigma = \frac{lf}{\xi}, \tag{A.8}$$

$$f = n_0R_a^{m_0}[1+(R_v/R_a)^2]^{(1+m_0)/2}, \quad B = 2-\frac{(R_v/R_a)^2-m_0}{(R_v/R_a)^2+1}, \tag{A.9}$$

$$E = \frac{1+\zeta}{2(1+\zeta+2\sigma)}, \quad R_a = \frac{2v\xi}{\eta}, \tag{A.10}$$

$$R_v = \frac{R_s\omega\xi}{\eta}. \tag{A.11}$$

Note that γ, K_s, C_s are nonlinear functions of x and y.

Appendix B. Evaluation of matrix T

The evaluation of transformation matrix, **T**, is given in Ref. [24] as follows:

$$\mathbf{T} = \exp(\mathbf{H}\tau) = [\exp(\mathbf{H}\tau/\bar{N})]^{\bar{N}}. \tag{B.1}$$

Selecting $\bar{N} = 2^N$ (if $N = 20$, $\bar{N} = 1,048,576$) and hence $\Delta t = \tau/\bar{N}$ is very small,

$$\exp(\mathbf{H}\Delta t) \approx \mathbf{I}+\mathbf{H}\Delta t+(\mathbf{H}\Delta t)^2/2+(\mathbf{H}\Delta t)^3/3!+(\mathbf{H}\Delta t)^4/4! = \mathbf{I}+\mathbf{T}_a, \tag{B.2}$$

where

$$\mathbf{T}_a = \mathbf{H}\Delta t+(\mathbf{H}\Delta t)^2[\mathbf{I}+(\mathbf{H}\Delta t)/3+(\mathbf{H}\Delta t)^2/12]/2. \tag{B.3}$$

Then

$$\mathbf{T} = (\mathbf{I}+\mathbf{T}_a)^{2^N}. \tag{B.4}$$

Note that $\mathbf{I}$ is the identity matrix and $\mathbf{T}_a$ is small in magnitude. In order to mitigate the possibility of the loss of numerical precision, the following expression is adopted in the computing implementation:

$$\mathbf{T} = (\mathbf{I} + \mathbf{T}_a)^{2^N} = (\mathbf{I} + \mathbf{T}_a)^{2^{N-1}} (\mathbf{I} + \mathbf{T}_a)^{2^{N-1}}. \tag{B.5}$$

References

[1] H.F. Black, E.A. Cochrane, Leakage and hybrid bearing properties of serrated seals in centrifugal pumps, *Proceedings of Sixth International Conference on Fluid Sealing*, Munich, German, 1973, pp. 61–70.

[2] D.W. Childs, Dynamic analysis of turbulent annular seals based on Hirs' lubrication equation, *Journal of Lubrication Technology* 105 (1983) 429–436.

[3] L.A. San Andres, Dynamic force and moment coefficients for short length annular seals, *Journal of Tribology* 115 (1993) 61–70.

[4] K. Kwanka, Dynamic coefficients of stepped labyrinth gas seals, *Journal of Engineering for Gas Turbine and Power* 122 (2000) 473–477.

[5] D. Eser, Rotordynamic coefficients in stepped labyrinth seals, *Computer Methods in Applied Mechanics and Engineering* 191 (2002) 3127–3135.

[6] D.W. Childs, J.K. Scharrer, Experimental rotordynamics coefficient results for teeth on rotor labyrinth gas seals, *NASA Conference Publication, Rotordynamic Instability Problems in High-Performance Turbomachinery* 2443 (1986) 259–275.

[7] K. Kwanka, M. Nagel, Experimental rotordynamic coefficients of short labyrinth gas seals, *NASA Conference Publication, Rotordynamic Instability Problems in High-Performance Turbomachinery* 3344 (1996) 135–144.

[8] T. Iwatsubo, Flow induced force and flow patterns of labyrinth seals, *NASA* cp-2250 (1982) 205–222.

[9] J.K. Scharrer, D.W. Childs, Theory vs. experiment for the rotordynamic coefficients of labyrinth gas seals, parts 1 & 2, *Journal of Vibration, Acoustics, Stress and Reliability in Design* 110 (1988) 270–287.

[10] C.H. Kim, Test results for rotordynamic coefficients of anti-swirl self-injection seals, *Journal of Tribology* 116 (1994) 508–513.

[11] A. Muszynska, Stability of whirl and whip in rotor/bearing systems, *Journal of Sound and Vibration* 127 (1988) 49–64.

[12] U. Yucel, Effects of Labyrinth Seals on the Stability of Rotors, PhD Thesis, Lehigh University, Bethlehem, PA, USA, 2000.

[13] O.R. Marquette, D.W. Childs, An extended three-control-volume theory for circumferentially grooved liquid seals, *Journal of Tribology* 118 (1996) 276–285.

[14] S.T. Noah, P. Sundararajan, Significance of considering nonlinear effects in predicting the dynamic behavior of rotating machinery, *Journal of Vibration and Control* 1 (1995) 431–458.

[15] A. Muszynska, Whirl and whip-rotor/bearing stability problems, *Journal of Sound and Vibration* 110 (1986) 443–462.

[16] A. Muszynska, Improvements in lightly loaded rotor/bearing and rotor/seal models, *Journal of Vibration, Acoustics, Stress and Reliability in Design* 110 (1988) 129–136.

[17] A. Muszynska, D.E. Bently, Frequency-swept rotating input perturbation techniques and identification of the fluid force models in rotor/bearing/seal systems and fluid handling machines, *Journal of Sound and Vibration* 143 (1990) 103–124.

[18] A. Muszynska, Fluid-related rotor/bearing/seal instability problems, Bently Rotor Dynamics Research Corporation Report, 1986.

[19] Y.S. Chen, Q. Ding, S.J. Hou, Stability and Hopf bifurcation of nonlinear rotor seal system, *Journal of Vibration Engineering* 10 (1997) 368–374.

[20] G. Adiletta, A.R. Guido, C. Rossi, Nonlinear dynamics of a rigid unbalanced rotor in journal bearings, part II: experimental analysis, *Nonlinear Dynamics* 14 (1997) 157–189.
[21] Q. Ding, J.E. Cooper, A.Y.T. Leung, Hopf bifurcation analysis of a rotor/seal system, *Journal of Sound and Vibration* 252 (2002) 817–833.
[22] J. Hua, Z.S. Liu, Q.Y. Xu, S. Swaddiwudhipong, A new high precision direct integration scheme for nonlinear rotor–seal system, *Proceedings of the International Conference on Scientific and Engineering Computation, Recent Advances in Computational Science and Engineering* (2002) 552–556.
[23] J. Hua, Nonlinear Dynamic Stability of Rotor-Bearing Systems, PhD Thesis, Xi'an Jiaotong University, PRC, 2002.
[24] W.X. Zhong, Precise computation for transient analysis, *Computational Structural Mechanics and Applications* 12 (1995) 1–6 (in Chinese).
[25] J.H. Lin, W.P. Shen, F.W. Williams, A high precision direct integration scheme for structures subjected to transient dynamic loading, *Computer and Structures* 56 (1995) 113–120.
[26] G. Iooss, D.D. Joseph, *Elementary Stability and Bifurcation Theory*, Springer, New York, 1989.
[27] R. Seydel, *From Equilibrium to Chaos, Practical Bifurcation and Stability Analysis*, Elsevier, Amsterdam, 1988.
[28] A. Wolf, J.B. Swift, L.H. Sweinney, J.A. Vastano, Determining Lyapunov exponents from a time series, *Physica D* 16 (1985) 285–317.